JTTEE5 19:207–218
DOI: 10.1007/s11666-009-9436-9
1059-9630/$19.00 © ASM International

Al_2O_3-ZrO_2 Finely Structured Multilayer Architectures from Suspension Plasma Spraying

Olivier Tingaud, Ghislain Montavon, Alain Denoirjean, Jean-François Coudert, Vincent Rat, and Pierre Fauchais

(Submitted April 23, 2009; in revised form October 2, 2009)

Suspension plasma spraying (SPS) is an alternative to conventional atmospheric plasma spraying (APS) aiming at manufacturing thinner layers (i.e., 10-100 μm) due to the specific size of the feedstock particles, from a few tens of nanometers to a few micrometers. The staking of lamellae and particles, which present a diameter ranging from 0.1 to 2.0 μm and an average thickness from 20 to 300 nm, permits to manufacture finely structured layers. Moreover, it appears as a versatile process able to manufacture different coating architectures according to the operating parameters (suspension properties, injection configuration, plasma properties, spray distance, torch scan velocity, scanning step, etc.). However, the different parameters controlling the properties of the coating, and their interdependences, are not yet fully identified. Thus, the aim of this paper is, on the one hand, to better understand the influence of operating parameters on the coating manufacturing mechanisms (in particular, the plasma gas mixture effect) and, on the other hand, to produce Al_2O_3-ZrO_2 finely structured layers with large varieties of architectures. For this purpose, a simple theoretical model was used to describe the plasma torch operating conditions at the nozzle exit, based on experimental data (mass enthalpy, arc current intensity, thermophysical properties of plasma forming gases, etc.) and the influences of the spray parameters were determined by mean of the study of sizes and shapes of spray beads. The results enabled then to reach a better understanding of involved phenomena and their interactions on the final coating architectures permitting to manufacture several types of microstructures.

Keywords Al_2O_3-ZrO_2, finely structured layer, microstructure, plasma gases, plasma torch, spray bead, suspension plasma spraying

1. Introduction

Since more than one decade, many works are devoted to the elaboration of finely structured layers by thermal spray technology. Indeed, due to the large volume fraction of the internal interfaces, coatings structured at the sub-micrometer scale should exhibit better properties than those, more conventional, structured at the micrometer one. They could hence offer pertinent solutions to numerous emerging applications, particularly for energy production, energy saving, diffusion and environmental barriers, etc. (Ref 1).

Among the different possible routes to produce finely structured layers, suspension plasma spraying (SPS) appears as one of the most versatile. Indeed, SPS is an alternative to conventional atmospheric plasma spraying (APS) to produce thinner layers (i.e., 10-100 μm) due to the smaller size of the feedstock particles, from a few tens of nanometers to a few micrometers. It consists in injecting within the plasma flow a suspension made of the feedstock particles, a liquid phase and a dispersant. Upon penetration within the d.c. plasma jet, two phenomena occur sequentially: droplet fragmentation and evaporation. Particles are then processed by the plasma flow prior to their impact, spreading and solidification upon the surface to be covered. The staking of resulting lamellae and particles (of characteristic diameters ranging from 0.1 to 2.0 μm and average thicknesses from 20 to 300 nm) permits to manufacture finely structured layers.

Indeed, SPS layers are made of well molten particles (*W*) forming flattened lamellae, unmolten particles (*U*) that exhibit the shape of the initial feedstock (that depends upon its manufacturing route) and corresponding to particles that have not traveled within the warm potential core of the plasma flow but rather in its colder fringes and small spherical grains corresponding to molten particles (i.e., to particles that have traveled within the warm

This article is an invited paper selected from presentations at the 2009 International Thermal Spray Conference and has been expanded from the original presentation. It is simultaneously published in *Expanding Thermal Spray Performance to New Markets and Applications: Proceedings of the 2009 International Thermal Spray Conference*, Las Vegas, Nevada, USA, May 4-7, 2009, Basil R. Marple, Margaret M. Hyland, Yuk-Chiu Lau, Chang-Jiu Li, Rogerio S. Lima, and Ghislain Montavon, Ed., ASM International, Materials Park, OH, 2009.

Olivier Tingaud, Ghislain Montavon, Alain Denoirjean, Jean-François Coudert, Vincent Rat, and **Pierre Fauchais**, SPCTS, UMR CNRS 6638, Faculty of Sciences and Technologies, University of Limoges, 123 Avenue Albert Thomas, 87060 Limoges cedex, France. Contact e-mails: olivier.tingaud@unilim.fr and ghislain.montavon@unilim.fr.

List of Symbols and Acronyms

Symbol	
I	arc current intensity (A)
V	electric arc average voltage (V)
ΔV	plasma torch instantaneous arc voltage fluctuation (V)
ΔP_{plasma}	reservoir relative isentropic pressure (Pa)
$\bar{h}$	specific enthalpy (MJ kg^{-1})
$\bar{u}$	plasma flow average velocity at torch exit (m s^{-1})
$\dot{m}$	plasma gas mass flow rate (kg s^{-1})
P_{th}	thermal losses in the plasma torch cooling circuit (W)
$c_p(T)$	specific heat at constant pressure (J kg^{-1} K^{-1})
v_{th}	thermal agitation velocity (m s^{-1})
ℓ	mean free path (m)
a_φ	coefficient depicting the ''quality'' of the thermal transfer (the higher the coefficient, the better the heat transfer) (kg m^{-1} s^{-1})
d	plasma torch exit diameter (m)
S	plasma torch exit cross-sectional area (m^2)
Pr	Prandtl number (dimensionless)

Greek Symbols	
γ	flow average isentropic coefficient (dimensionless)
$\varphi(T)$	plasma flow average heat potential (W m^{-1})
$\kappa(T)$	plasma flow average thermal conductivity (W m^{-1} K^{-1})
$\sigma(T)$	plasma flow average electrical conductivity (S m^{-1})
φ_s	average heat flux imparted by plasma flow to the substrate (W m^{-2})
ρ	plasma flow average specific mass (kg m^{-3})
υ	plasma flow average kinematic viscosity (m^2 s^{-1})
α	plasma flow average thermal diffusivity (m^2 s^{-1})

Abbreviations	
NP	number of passes of plasma torch in front of the substrate (number)
MP	suspension mass percentage (%)
SV	torch relative scanning velocity (m s^{-1})
SS	deposition scanning step (mm per pass)
SD	spray distance (mm)

plasma core) that have resolidified (R) prior to their impact upon the substrate (i.e., that these particles have been ejected from the plasma potential core, very likely due to thermophoresis effect, and that have resolidified in the fringes due to their poor thermal inertia; Ref 2, 3). By estimating the fraction of poorly treated particles embedded in the coating ($P = U + R$) to the fraction of well melted particles W, a $T = P/W$ qualitative ratio of particle treatment can be defined as a function of operating parameters. An evolution of the T ratio leads to an evolution of the coating architecture. Indeed, the higher the T ratio, the higher the density of stacking defects and so the higher the coating void content (Ref 4).

Nevertheless, even if the effects of some operating parameters, such as the influence of the particle size distribution and their morphologies (Ref 5), are well known, the interdependences of parameters controlling the coating architecture, including power and kinematics parameters are not yet fully identified. Therefore, it appears that the optimization of the process requires a better understanding of involved phenomena and their interactions.

To reach this objective, an online control system is required to characterize the whole process in order to systematically operate the spray system under the same conditions and determine much easily the influence of spray parameters. It appears indeed that the properties of the plasma jet are among the most important parameters of the SPS process as they control the fragmentation of the suspension stream and the processing of particles. Coudert and Rat (Ref 6) have suggested a simple theoretical model in order to characterize the plasma flow at the nozzle exit of a d.c. plasma torch operating at atmospheric pressure according to (for a fixed torch configuration) its specific enthalpy and the thermophysical properties of the plasma forming gases. This model has been used in this work to describe the plasma torch working conditions enabling to operate in the same conditions between experiments. This control associated with the study of the evolution of size and shape of spray beads according to the operating conditions (Ref 4, 7-9) permits to determine the influence of some spray parameters on the structure of the coating.

Al_2O_3-ZrO_2 composite coatings were considered for a demonstrative purpose: due to its thermophysical properties, particularly its latent heat of melting and its average specific heat (1092 kJ kg^{-1} and 753 J kg^{-1} K^{-1}, respectively), Al_2O_3 is far more difficult to process by a plasma flow (i.e., to melt particles of identical weights) than ZrO_2 (latent heat of melting of 706 kJ kg^{-1} and average specific heat of 450 J kg^{-1} K^{-1}); meanwhile, it exhibits a higher melting temperature (2715 °C to be compared to 2054 °C for Al_2O_3). Spraying such composite coatings requires hence a very specific optimization of operating parameters.

2. Analytical Model

The simplified approach suggested by Coudert and Rat (Ref 6) attempts to highlight the influence of experimental parameters on plasma flow properties. In this model, it is indeed assumed that the plasma flow, at the nozzle exit, behaves such as an isentropic flow which would exit from a reservoir.

The arc column is where the electrical energy of the power source is converted into thermal and, to a less extend, kinetic energies. The electrical power supplied to the torch after removing the heat losses in the cooling circuit is so supposed to be converted into an enthalpic flux. Neglecting the kinetic energy of the plasma flow, which represents only a few percents of the total energy in usual operating conditions, an equivalent specific enthalpy $\bar{h}$ (MJ kg^{-1}) can be defined as follows:

$$\bar{h} = \frac{U \times I - P_{th}}{\dot{m}} \quad \text{(Eq 1)}$$

where U, I, and P_{th} are the measured mean values of the arc voltage (V), the arc current intensity (A), and the torch thermal losses (W), respectively, whereas $\dot{m}$ corresponds to the mass flow rate (kg s^{-1}) of the plasma forming gases.

Assuming the local thermodynamic equilibrium (LTE), the different thermodynamic characteristics such as the specific heat at constant pressure, $c_p(T)$ (J kg^{-1} K^{-1}), the thermal conductivity, $\kappa(T)$ (W m^{-1} K^{-1}), the electrical conductivity, $\sigma(T)$ (S m^{-1}), the heat potential, $\varphi(T)$ (W m^{-1}), etc. can be expressed as a function of temperature. Thus, Eq 2 and 3 correlate the specific enthalpy to the temperature by means of the specific heat and the heat potential to the temperature by means of the thermal conductivity, respectively, as follows:

$$h(T) = h_{ref} + \int_{T_{ref}}^{T} c_p(T) \cdot dT \quad \text{(Eq 2)}$$

$$\varphi(T) = \varphi_{ref} + \int_{T_{ref}}^{T} \kappa(T) \cdot dT \quad \text{(Eq 3)}$$

Although the kinetic gas theory permits to establish a simple correlation, however approximate, between $\kappa(T)$ and $c_p(T)$ as follows:

$$\kappa(T) = \frac{1}{3} \times \rho \times c_p \times \nu_{th} \times \ell \quad \text{(Eq 4)}$$

where $\kappa(T)$ is the gas thermal conductivity (W m^{-1} K^{-1}), ρ its specific mass (kg m^{-3}), ν_{th} the thermal agitation velocity (m s^{-1}) and ℓ the mean free path (m).

The heat potential $\varphi(T)$ (Eq 3) shows almost the same evolution with temperature than the specific enthalpy $h(T)$ (Eq 2), as depicted for example in Fig. 1 for an Ar-H_2 (45-15 L min^{-1}) plasma gas mixture and can be hence linearized as follows:

$$\varphi(T) = a_\varphi \times \bar{h}(T) + b_\varphi \quad \text{(Eq 5)}$$

where a_φ and b_φ are constants that are numerically adjusted as a function of the considered plasma gases.

Thus, the slope of the curve $\varphi = f(\bar{h})$ is directly linked to the gas thermal conductivity through the a_φ coefficient representative of the ''quality'' of the thermal transfer: the higher the a_φ coefficient, the higher the thermal transfer. Figure 2 shows that for the same specific enthalpy, an Ar-H_2 plasma gas mixture is characterized by a heat potential higher than an Ar-He mixture. This means that

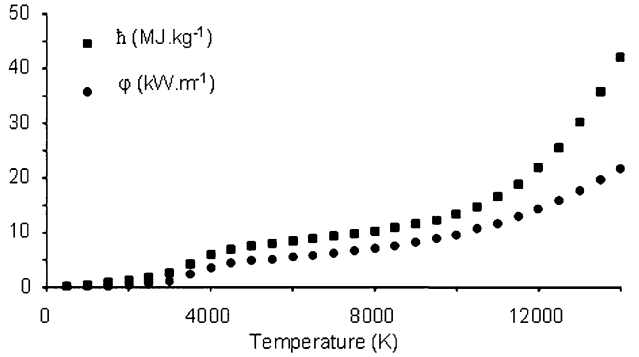

Fig. 1 Specific enthalpy and heat potential vs. temperature for an Ar-H_2 (45-15 L min^{-1}) plasma gas mixture

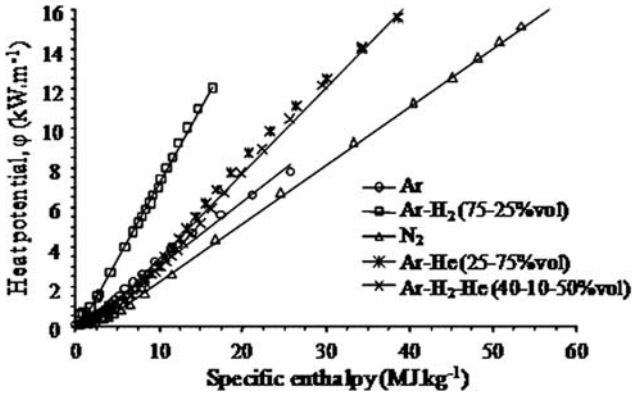

Fig. 2 Heat potential evolution vs. specific enthalpy for different experimental conditions

Table 1 Thermophysical properties for different plasma gas mixtures at the atmospheric pressure

Plasma gas mixture	$\bar{h}$, MJ kg^{-1}	a_φ, 10^{-4} kg m^{-1} s^{-1}
Ar	3.70	3.06
Ar-H_2 (75-25 vol.%)	10.40	7.06
N_2	41.10	2.82
Ar-He (25-75 vol.%)	13.20	4.33
Ar-H_2-He (40-10-50 vol.%)	12.14	4.31

the thermal transfer ''quality'' is better for an Ar-H_2 plasma than for the others. Some values of a_φ for different plasma gases are reported in Table 1.

Since this simplified analytical model assimilates the real plasma flow to an isentropic flow exiting from a reservoir, the Barré de Saint Venant equation permits to depict the mean velocity, $\bar{u}$ (m s^{-1}) of the plasma flow at the nozzle exit as follows:

$$\frac{1}{2}\bar{u}^2 + \frac{\gamma}{\gamma - 1}\frac{P_a}{\bar{\rho}} = \bar{h} \quad \text{(Eq 6)}$$

where P_a is the atmospheric pressure (Pa) and γ the dimensionless isentropic coefficient of the gas mixture.

Besides, from the expression of the volume flow rate exiting the plasma torch ($m^3\ s^{-1}$), the following equation can be derived:

$$\rho \times \bar{u} = \frac{4 \times \dot{m}}{\pi \times d^2} \quad \text{(Eq 7)}$$

where d represents the plasma torch exit diameter (m).

Substituting Eq 7 into 6 leads to the following equation:

$$\bar{u}^2 + \frac{2\gamma \times P_a \times S}{(\gamma - 1) \times \dot{m}} \cdot \bar{u} - 2\bar{h} = 0 \quad \text{(Eq 8)}$$

where S represents the plasma torch exit cross-sectional area (m^2).

Equation 8 yields a very simple relationship for the plasma jet velocity and after some development (Ref 6), the flow mean velocity can be estimated as follows:

$$\bar{u} = \bar{h} \times \frac{\dot{m} \times (\gamma - 1)}{P_a \times S \times \gamma} = \frac{(U \times I - P_{th}) \times (\gamma - 1)}{P_a \times S \times \gamma} \quad \text{(Eq 9)}$$

Equation 9 accounts for the amount of thermal energy converted into kinetic energy through the ratio $(\gamma - 1)/\gamma$, where γ is an averaged isentropic exponent (dimensionless) which is directly linked to the plasma enthalpy or the ionization degree, as shown by Burm et al. (Ref 10). This model correlating $\bar{u}$ and $\bar{h}$ and the different operating conditions has been confirmed in previous works (Ref 11).

Consequently, the isentropic coefficient γ evolves with the selected plasma gas mixture. It describes the gas hydrodynamic effort. The gas impulsion, $\gamma - 1$, corresponds according to Feinman to the fraction of the internal energy converted into mechanical energy. Thus, a small variation of γ leads to a high variation of the gas impulsion. For example, a variation of the isentropic coefficient from 1.1 to 1.2 (a variation of ''only'' about 9%) leads to a variation of the gas impulsion from 0.1 to 0.2, that is an increase of 100%!

Besides, the isentropic overpressure ΔP_{plasma} (Pa) provided to the plasma flow is expressed as follows:

$$\Delta P_{plasma} = \frac{\gamma - 1}{2\gamma} \frac{\dot{m}^2 \times \bar{h}}{P_a \times S^2} \quad \text{(Eq 10)}$$

The slope of the curve $\Delta P_{plasma} = f\left(\frac{\dot{m}^2 \times \bar{h}}{P_a \times S^2}\right)$, permitting to describe the operating parameters effect on the isentropic overpressure, allows then determining this averaged isentropic exponent. Previous measurements (Ref 6) confirmed the validity of Eq 10. For example, for an Ar-H_2 (75-25 vol.%) plasma gas mixture, the data series permitted to estimate the isentropic coefficient of the mixture within the 1.15-1.20 range.

Finally, the heat flux, φ_s ($W\ m^{-2}$), transferred by the plasma jet to the substrate depends upon the specific enthalpy, the thermal boundary layer thickness at the stagnation point and the plasma gas mixture thermophysical properties. Thus, a simplified relationship correlating the thermal flux imparted by the plasma flow to a substrate placed perpendicularly to the flow direction to the operating conditions can be estimated as follows (Ref 12):

$$\varphi_s = a_\varphi \times \sqrt{\frac{Pr}{\upsilon} \times \bar{h} \times \sqrt{\frac{\bar{u}}{SD}}} \quad \text{(Eq 11)}$$

where Pr is the dimensionless Prandtl number corresponding to the ratio of the kinematic viscosity, υ ($m^2\ s^{-1}$), to the thermal diffusivity, α ($m^2\ s^{-1}$), and SD is the spray distance (m).

Substituting Eq 9 into 11 permits to estimate the heat flux imparted by the plasma flow to the substrate as follows:

$$\varphi_s \approx a_\varphi \sqrt{\frac{Pr}{\upsilon}} \times \bar{h}^{3/2} \times f(SD) \quad \text{(Eq 12)}$$

where f(SD), a function of the spray distance, can be only estimated by a more complex calculation taking into account the plasma flow properties (Ref 12).

Equation 12, which remains an approximated relationship, underlines nevertheless the importance of the specific enthalpy and the plasma gas properties on the heat transfer imparted to the substrate by the plasma flow through the $\left(a_\varphi \times \sqrt{\frac{Pr}{\upsilon}} \times \bar{h}^{3/2}\right)$ term. Its evaluation is obtained from transport coefficients of the plasma gas mixture. This relationship has been successfully tested by Etchart-Salas (Ref 12, 13). Indeed, experimental measurements for several plasma gas mixtures indicated a sharp decrease in the transferred heat flux as a function of the spray distance (in front of the effect of the nature of the plasma gas mixture) which attests of the plasma jet thinning in its surrounding environment.

Thus, the suggested simplified analytical model allows describing the main properties of the plasma flow at the nozzle exit. It does not provide nevertheless the absolute values of the different plasma characteristics neither it describes the electric arc physic. It permits however to depict relative trends and orders of magnitude of effects of experimental parameters enabling to conduct reliable comparisons, to work in the same conditions between several experiments and to understand much easily the influence of the spray parameters. This approach has been implemented systematically in the following.

3. Experimental Setups

Suspensions of alumina and zirconia were respectively made of angular single monocrystalline α-Al_2O_3 (P152 SB, Alcan, Saint-Jean de Maurienne, France) of 0.5 µm average diameter (d_{50}) and ZrO_2-001H powder (Unitec Ceramic, Stafford, UK) of $d_{50} = 0.036$ µm. The two powders were dispersed into pure ethanol with an electrosteric dispersant. The powder mass fraction in suspensions was varied from 5 to 20%. Prior to spraying, the suspensions were sonicated for 5 min.

A stick-cathode d.c. plasma torch developed in house and equipped with a 5 mm internal diameter nozzle was

implemented for experiments. It was operated with different plasma forming gas mixtures (Ar-He 30-30 L min^{-1}, Ar-H_2 45-15 L min^{-1} and Ar-He-H_2 30-30-5 L min^{-1}) with an arc current intensity varying from 300 to 600 A.

Several measurements according to the analytical model were performed to characterize the plasma flow at the nozzle exit, all along the experiments. Thus, the arc voltage, the arc current intensity, the heat losses in the cooling circuit, the plasma gas mass flow rate, and the isentropic overpressure were recorded. The instantaneous arc voltage was also recorded using a digital oscilloscope. The spray torch scan velocity was fixed to 1 m s^{-1} according to previous work (Ref 4). The spray distance was varied from 30 to 50 mm. The substrate temperature, measured by infrared pyrometry (8-14 μm wavelength range), evolved from 250 and 600 °C during spraying. Thanks to the high mechanical compliance of the layers induced very likely by the sub-micrometer-sized particles, no crack nor delamination through the layers has been ever observed meanwhile such a high temperature after spraying. Table 2 displays the principal operating parameters that were used. Table 3 displays the main characteristics of the plasma flow. The isentropic overpressures ΔP_{plasma} correspond to measurements made on the plasma gas feeding line, just before the injection in the electric arc chamber. The specific enthalpies, $\bar{h}$, were calculated by Eq 1. The isentropic coefficients, γ, were deduced from the slops of the $\Delta P_{plasma} = f(\dot{m}^2 \times \bar{h})$ fitted lines. The plasma flow average velocities, $\bar{u}$, were calculated from Eq 9. Finally, the heat flux densities, φ_s, were calculated as a function of the measured specific enthalpies, $\bar{h}$, and correlations with anterior flux measurements performed in the laboratory (Ref 12). For these calculations, the a_φ coefficients correspond to the slopes of fitted lines depicted in Fig. 2 and reported in Table 1.

Spray beads (Ref 4) were sprayed onto 316L stainless steel plates (120 × 50 × 5 mm^3) that were previously degreased by immersion in acetone vapors and prepolished using SiC papers and polished using diamond slurries to obtain an average roughness, R_a, of about 0.1 μm, average value. Coatings were sprayed onto 316L stainless steel buttons (25 mm in diameter and 20 mm in thickness) exhibiting a similar average roughness.

The spray bead profiles and their surface average roughness were assessed using a diamond stylus profilometer (Dektak IIA surface profilometer, Sloan Technology, Santa Barbara, CA). Ten radial measurements randomly located along the spray bead were carried out on each sample. After adjustment (by discarding the highest and the lowest values), data were averaged. Gaussian functions were selected to fit, with correlation factors ranging from 0.95 to 0.99, the spray bead profiles. Additional size and shape factors were defined, such as the spray bead cross-sectional area A (m^2) representative of the intrinsic deposition efficiency, the spray bead width (mm) and height H (μm) and its width at half-height W (mm) which permitted to define an optimized scanning step (Ref 4).

Table 2 Major operating parameters

Suspension	
Alumina mass ratio [MP], %	5-20
Dispersant	Electrosteric (Beycostat C213)
Liquid phase	Et-OH (99.5%)
Suspension injection	
Injector internal diameter, μm	150
Reservoir relative pressure, MPa	0.2-0.5
Particles mass rate, g min^{-1}	0.75-6.00
Plasma torch operating parameters	
Type	Stick mono cathode
Anode internal diameter at plasma torch exit, mm	5
Argon primary plasma forming gas [Ar], L min^{-1}	30/30/45
Helium secondary plasma forming gas [He], L min^{-1}	30/30/0
Hydrogen secondary plasma forming gas, L min^{-1} [H_2]	0/5/15
Arc current intensity [I], A	300-600
Plasma torch instantaneous arc voltage relative fluctuations [$\Delta V/V$]	Ar-He 30-30 L min^{-1}: $\Delta V/V$ ~ 0.2 Ar-He-H_2 30-30-5 L min^{-1}: $\Delta V/V$ ~ 0.4 Ar-H_2 45-15 L min^{-1}: $\Delta V/V$ ~ 0.7
Plasma flow average mass enthalpy [$\bar{h}$], MJ kg^{-1}	10-16
Spray torch scan velocity [SV], m s^{-1}	1
Spray distance [SD], mm	30-50
Scanning step [SS], mm per pass	10 mm (for coating)
Number of passes [NP], –	Variable depending experiment

Table 3 Main properties of the plasma flow for different plasma gas mixtures and operating conditions

Plasma gas mixture, L min^{-1}	*I*, A	ΔP_{plasma}, MPa	$\bar{h}$, MJ kg^{-1}	γ, –	$\bar{u}$, m s^{-1}	φ_s, MW m^{-2}	$\Delta V/V$, –
Ar-He [30-30]	500	0.544	15.4	1.40	2239	12.0	0.2
	400	0.422	12.2		1774	8.2	
	300	0.327	9.1		1323	5.0	
Ar-He-H_2 [30-30-5]	500	0.545	18.2	1.30	2117	18.8	0.4
	400	0.458	14.9		1733	13.9	
	300	0.362	11.0		1279	8.8	
Ar- H_2 [45-15]	500	0.626	20.5	1.15	1879	36.7	0.7
	400	0.532	18.0		1650	30.2	
	300	0.423	14.0		1283	20.7	

4. Results and Discussion

4.1 Plasma Torch Operating Conditions

Figure 3, representing the evolution of $\Delta P_{plasma} = f(\dot{m}^2 \cdot \bar{h})$ of carried out experiments, shows that the averaged isentropic coefficient is higher for an Ar-He ($\gamma = 1.40$) plasma gas mixture than for Ar-H_2 ($\gamma = 1.15$, value in good correlation with data published in Ref 6) or Ar-He-H_2 ($\gamma = 1.30$) ones. Consequently, at identical specific enthalpies or plasma gas flow rates, an Ar-He plasma gas mixture produces a plasma flow with higher velocity than an Ar-H_2 mixture and the addition of H_2 leads to the decrease in the ''quality'' of the dynamic transfer. From Eq 9, the mean velocity of the plasma flow at the nozzle exit, $\bar{u}$, can be evaluated. The γ and $\bar{u}$ values for different operating conditions are reported in Table 3, together with φ_s values for different operating conditions at a spray distance of 40 mm. It clearly appears that the heat flux transferred from the plasma flow to the substrate is very high, particularly with an Ar-H_2 plasma gas mixture where φ_s reach values as high as 30 MW m^{-2} (this is more than one order of magnitude higher than the one imparted in conventional APS at a spray distance of about 100 mm). Moreover, together with such high heat fluxes are associated high transitional temperatures due, on the one hand, to the interaction between the plasma flow and the substrate (interaction time, ΔT_i, of about 10^{-2} s according to the spray torch scan velocity) and, on the other hand, to the impact of molten particles (interaction time, ΔT_i, of about 10^{-6} s), leading very locally to the increase in the temperature from 400 to above 1000 °C (Ref 12). One can suppose that this thermal load could keep locally the deposited particles in a molten or semi-molten state resulting in a modified kinetics of solidification and ultimately in the formation of denser coatings. This assumption is evidenced in Fig. 4 showing the top view of a SPS

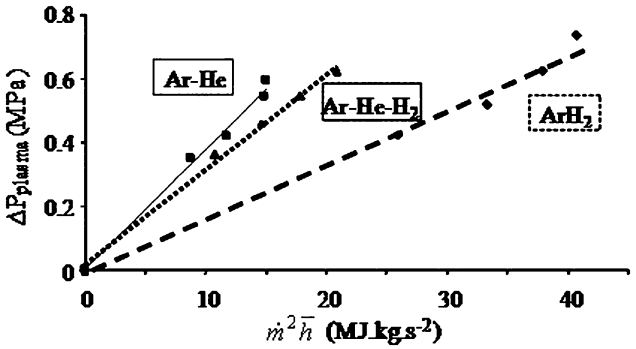

Fig. 3 Plasma overpressure for different plasma gas mixtures according to the spray conditions

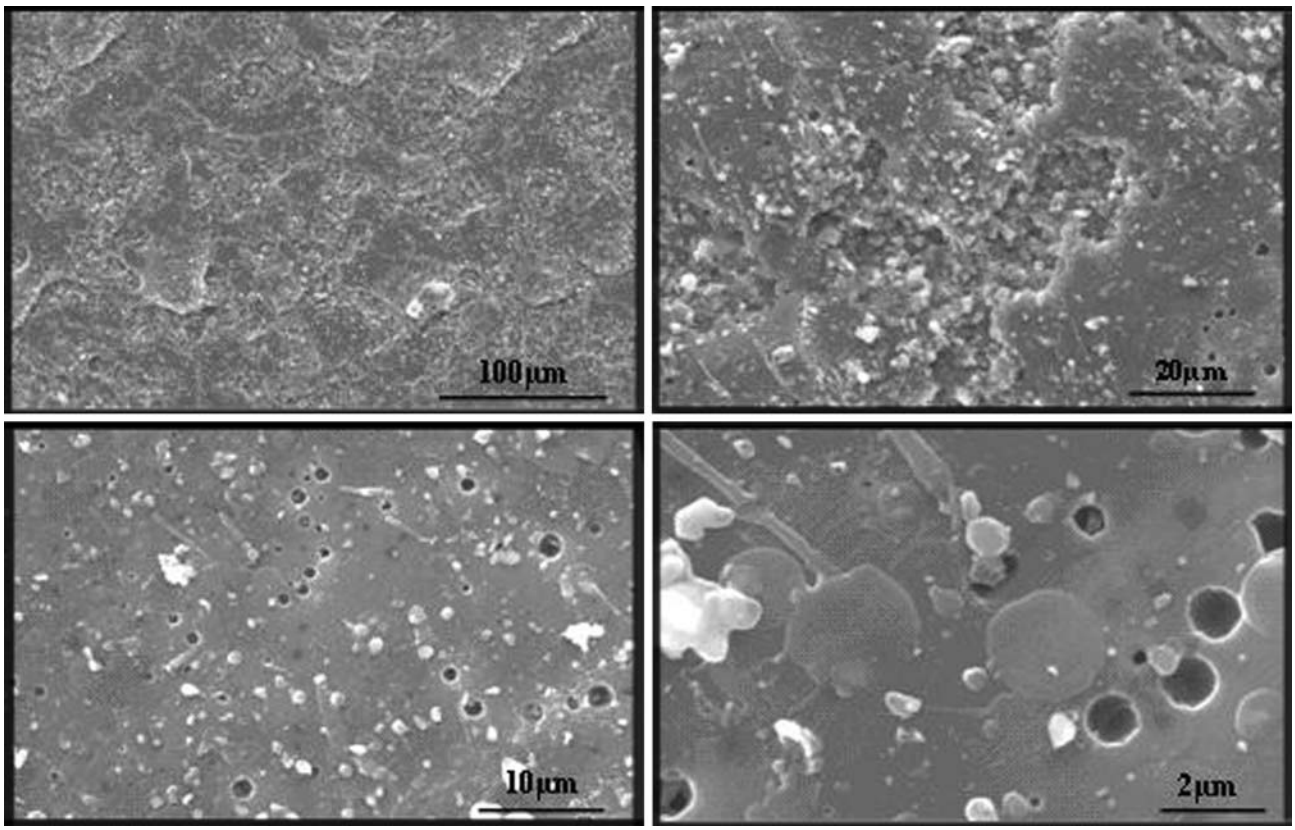

Fig. 4 SPS Al_2O_3 coating upper surface remelted by the plasma jet during coating manufacturing (Ar-H_2, $\bar{h} = 14$ MJ kg^{-1}, SV = 1 m s^{-1}, SD = 20 mm, NP = 76, SS = 10 mm)

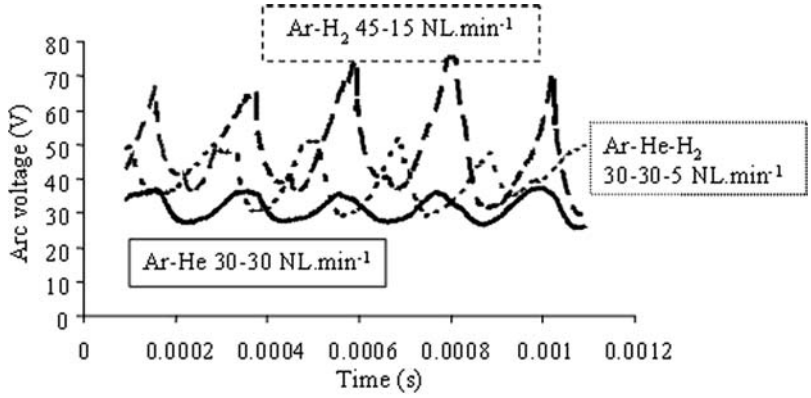

Fig. 5 Arc voltage fluctuations for several plasma gas mixtures

alumina coating (Ar-H_2 45-15 NL min^{-1}, $\bar{h} = 14$ MJ kg^{-1}, spray torch scan velocity (SV): 1 m s^{-1}, spray distance (SD) $\approx$ 20 mm, number of passes (NP): 76, scanning step (SS): 10 mm) where the deposited material has been remelted by the passage of the plasma torch.

The arc voltage fluctuations for the different plasma gas mixtures (see Table 3) are reported in Fig. 5. For all considered plasma compositions, the fluctuation frequency is around 5 kHz. The Ar-H_2 (45-15 NL min^{-1}) plasma flow shows an amplitude of variation, $\Delta V/V$, of 0.7. One can assume that due to such fluctuations, the suspension will be inhomogeneously processed. Indeed, the available energy in the plasma flow is fluctuating together with the plasma velocity, so that the different steps in suspension processing (suspension fragmentation, liquid phase vaporization, and solid particles melting and acceleration) are not achieved at the same rates all along the time of flight of the feedstock. *A contrario*, the Ar-He (30-30 L min^{-1}) plasma flow presents a fairly low variation of the instantaneous arc voltage ($\Delta V/V = 0.2$), leading very likely to a more homogeneous processing of suspension droplets. The Ar-He-H_2 ternary plasma gas mixture (30-30-5 L min^{-1}) which combines the properties of the two additional plasma gases (H_2 and He) shows a variation of the instantaneous arc voltage around 0.4.

4.2 Evolution of the Coating Architecture According to the Operating Conditions

As shown in Fig. 6, the spray bead evolution varies according to the plasma gas mixtures.

The deposited thickness decreases when changing the Ar-He plasma gas mixture to an Ar-H_2 and to the ternary composition ones. However, this reduction is not due to a sudden decrease in the intrinsic deposition efficiency but, as shown in Fig. 7, to an evolution of the spray bead microstructure. Indeed, the Ar-He plasma flow is characterized by an efficient kinetics transfer due to a higher viscosity together with high isentropic coefficient and average velocity. This leads to the formation of a homogeneous but relatively porous structure compared with the other plasma mixture compositions. An Ar-H_2 plasma flow, exhibiting a high heat potential, allows the

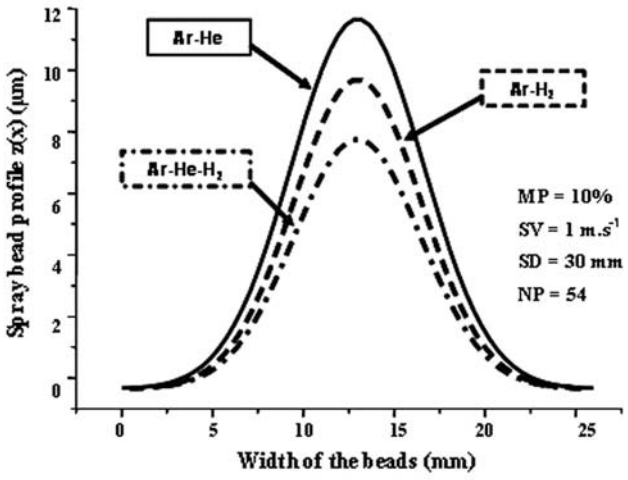

Fig. 6 Spray bead cross-sectional profile evolution according to the plasma gas mixture

manufacturing of a thin and dense bead at low spray distance. Finally, an Ar-He-H_2 plasma flow leads the formation of a dense bead thinner than those manufactured using the other mixture compositions. Moreover, the use of the ternary mixture allows very likely the homogenization of the suspension processing whatever its solid particle mass ratio (MP = 5, 10, or 20%) (Fig. 8). This figure shows that the thickness of the deposited material is very dependent upon the solid particle mass ratio and the selected plasma gas mixture. Thus, the spray beads manufactured using an Ar-He-H_2 plasma gas mixture, for low particle mass percentages in the suspensions (MP = 5 and 10%), show profiles of similar characteristics. At a higher mass percentage (MP = 20%), the thickness of the deposited material very largely increases for the two considered plasma compositions. Finally, one can note that the bead thickness is higher for MP = 5% than for MP = 10% when using an Ar-He plasma gas mixture. This is due, as shown in a previous study (Ref 4), to an evolution of the spray pattern dispersion angle which increases at MP = 5 and 20% (maximum value at 5%) and reaches a minimum at

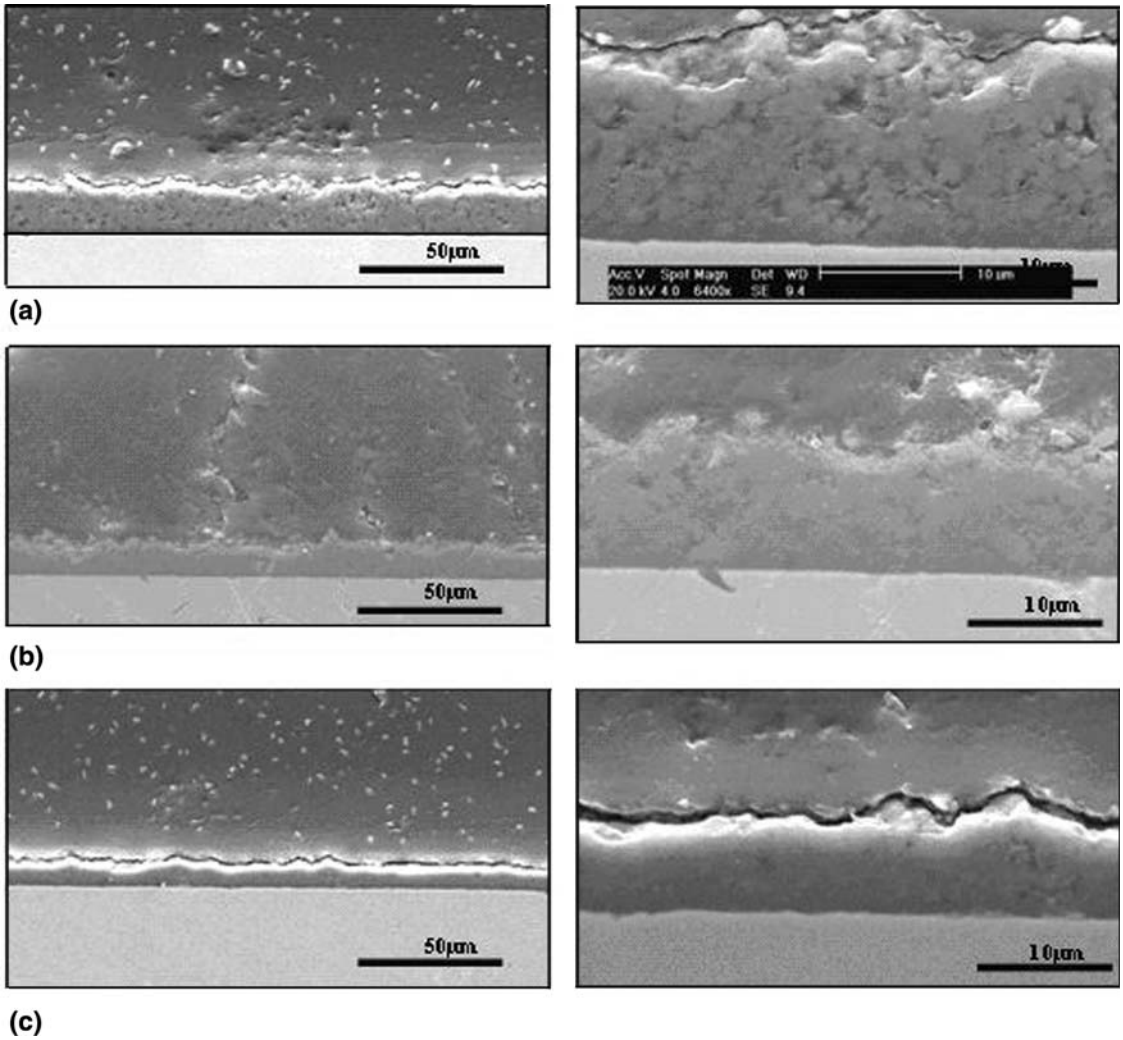

Fig. 7 Spray bead microstructure evolution according to the plasma gas mixture (MP = 10%, SD = 30 mm, SV = 1 m s^{-1}, NP = 54). (a) Ar-He 30-30 L min^{-1}, $\bar{h}$ = 10.5 MJ kg^{-1}. (b) Ar-H_2 45-15 L min^{-1}, $\bar{h}$ = 12 MJ kg^{-1}. (c) Ar-He-H_2 30-30-5 L min^{-1}, $\bar{h}$ = 15 MJ kg^{-1}

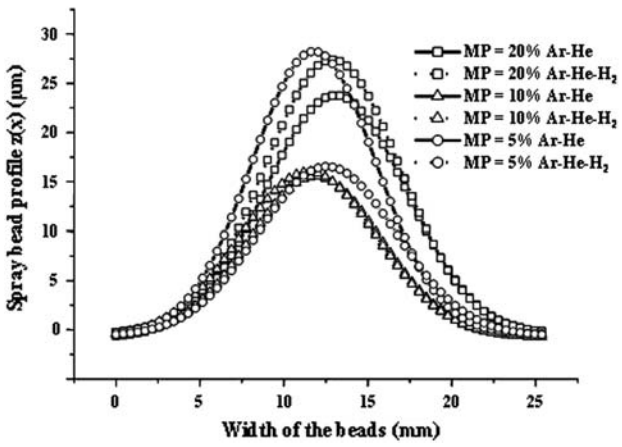

Fig. 8 Spray bead cross-sectional profile evolution for different mass percentages of solid particles in suspension (MP = 5, 10, and 20%) and different plasma gas mixtures (Ar-He 30-30 L min^{-1}, $\bar{h}$ = 11 MJ kg^{-1} and Ar-He-H_2 30-30-5 L min^{-1}, $\bar{h}$ = 15.5 MJ kg^{-1}, SD = 40 mm, SV = 1 m s^{-1}, NP = 76)

MP = 10%. At such a value, the particles undergo hence a better treatment by the plasma jet, whereas at MP = 5 or 20%, the particle processing becomes more heterogeneous and the fraction of poorly treated particles (*R* and *U*) embedded within the deposited material increases, leading to a more porous and less cohesive structure. A more porous structure corresponds to a lower apparent density and in turn to a thicker spray bead. However, as show in Fig. 9, and contrary to the use of an Ar-He plasma gas mixture that leads to a porous and poorly cohesive coating structure, the use of a ternary one permits the formation of a relatively dense and cohesive structure. These results confirm hence the importance of the nature of the plasma gas mixture on coating microstructure, in particular, through their ability to transfer their energy.

Indeed, the use of an Ar-He plasma gas mixture, even if it shows a high average gas impulsion, $\gamma - 1 \approx 0.40$, leading to an efficient kinetics transfer to the particles, does not permit to manufacture very dense coatings due to

his low specific enthalpy ($\bar{h} \approx 12$ MJ kg^{-1}) and its poor capability to transfer its thermal energy through the a_φ coefficient equal to 4.33×10^{-4} kg m^{-1} s^{-1}. In contrast, for an Ar-H_2 plasma mixture, the plasma/particles thermal transfer is much higher ($a_\varphi = 7.06 \times 10^{-4}$ kg m^{-1} s^{-1}) and leads to the manufacturing of denser coating microstructures. However, as shown in Fig. 10, at higher spray distance, the process becomes very sensitive to the instabilities induced by the arc voltage fluctuations ($\Delta V/V = 0.7$): heterogeneities within the structure increase due to the increase of poorly treated particles (R, U).

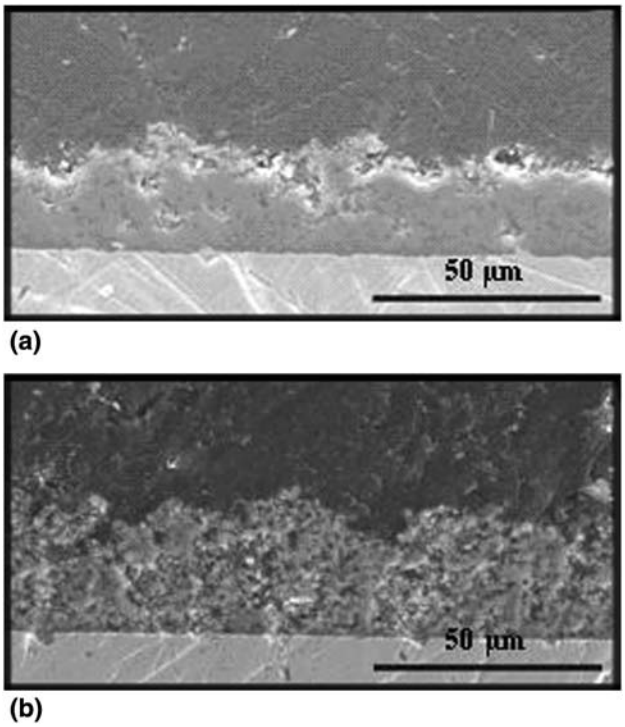

Fig. 9 Comparison between two SPS alumina coating microstructures: (a) Ar-He-H_2, 30-30-5 L min^{-1}, $\bar{h} = 15.5$ MJ kg^{-1}, (b) Ar-He 30-30 L min^{-1}, $\bar{h} = 11$ MJ kg^{-1} (MP = 20%, SD = 40 mm, SV = 1 m s^{-1}, NP = 76)

At last, it seems that the use of a ternary plasma gas mixture leads to a more homogeneous and efficient processing of the suspension, combining a high velocity, a high viscosity, and a longer plasma jet (avoiding thus the particles to be ejected from the plasma flow) associated with a high heat transfer (H_2) and a high specific enthalpy ($\bar{h} \approx 15$ MJ kg^{-1}) together with an acceptable arc voltage fluctuation ($\Delta V/V = 0.4$). So the use of such a plasma gas mixture should lead to the manufacturing of a dense structure, limiting the presence of poorly treated particles (R, U) within the coating.

4.3 Finely Structured Layers with Multiple Architectures

Thus, the aforementioned results permit to better understand some process manufacturing mechanisms and to clearly define trends permitting to adjust operating parameters to manufacture in a reproducible way coatings with various pore levels, with a pore gradient along the thickness or with different compositions. For example, Fig. 11 to 13 present three types of Al_2O_3-ZrO_2 coating characterized by different architectures; that is, a graded coating in term of composition, a composite coating, and a multilayer coating, respectively.

As already mentioned, layers architecture depends upon interrelated operating parameters effects, in particular (i) heat and momentum transfers to particles (related to plasma gas mixtures leading to different qualities of thermal transfer through the a_φ coefficient and different arc voltage fluctuations), (ii) particles momentum and thermal inertia (related to particle size and spray distance), (iii) heat flux imparted by plasma flow to substrate and previously deposited particles (φ_s value).

The relative effect of each operating parameters depends upon their combination. Consequently, the fraction of poorly treated particles is very dependent upon the combination of operating parameters.

Graded Al_2O_3-ZrO_2 coatings with two porous levels (Fig. 11) have been manufactured by spraying successively suspensions of variable compositions with an Ar-He plasma gas mixture (30-30 L min^{-1}, $\bar{h} = 12$ MJ kg^{-1}) at a 30 mm spray distance. The denser coating (Fig. 11a) has been manufactured with a narrow powder particle size distribution ($d_{90} - d_{10} = 420$ nm, $d_{50} \approx 400$ nm), whereas

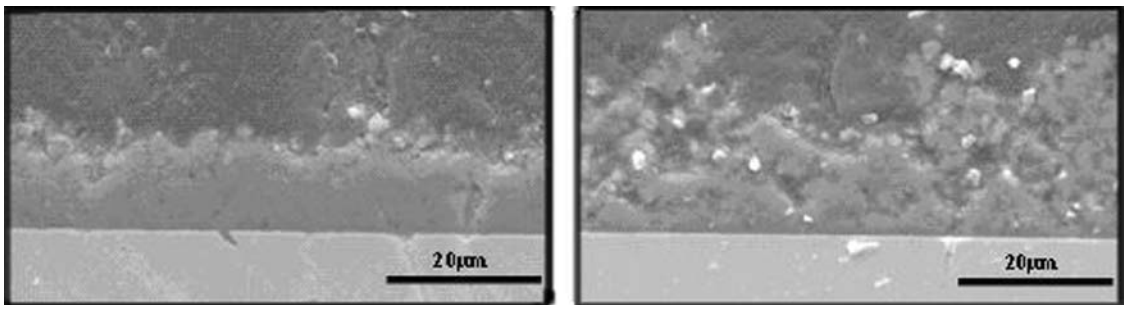

Fig. 10 Evolution of the coating microstructure according to the spray distance for an Ar-H_2 plasma gas mixture: (a) SD = 30 mm, (b) SD = 40 mm

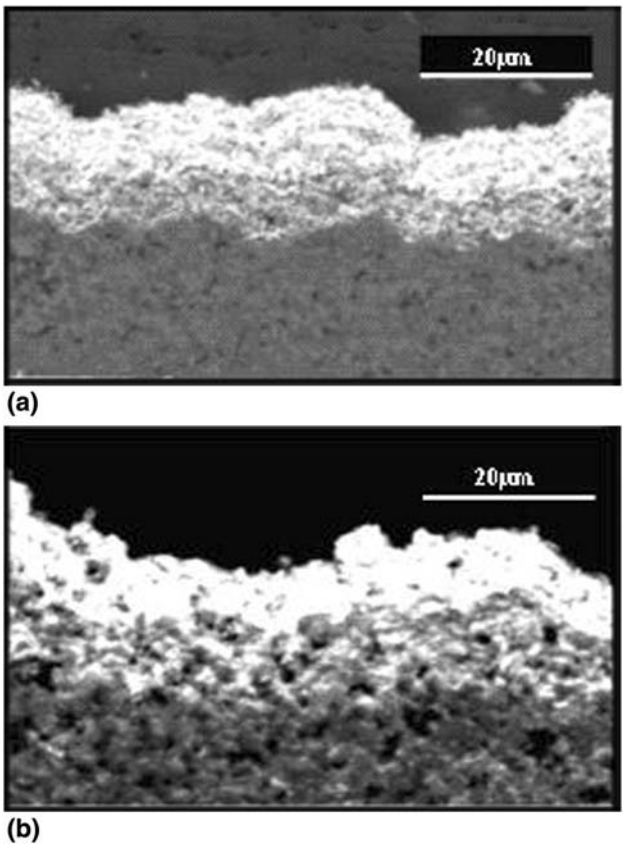

Fig. 11 Al_2O_3-ZrO_2 graded layers manufactured with Ar-He plasma gas mixture (30-30 L min^{-1}, $\bar{h} = 12$ MJ kg^{-1}, SD = 30 mm, SV = 1 m s^{-1}, MP = 10%) showing different microstructures according to the particle size distribution: (a) $d_{90} - d_{10} = 420$ nm ("dense"). (b) $d_{90} - d_{10} = 1270$ nm ("porous")

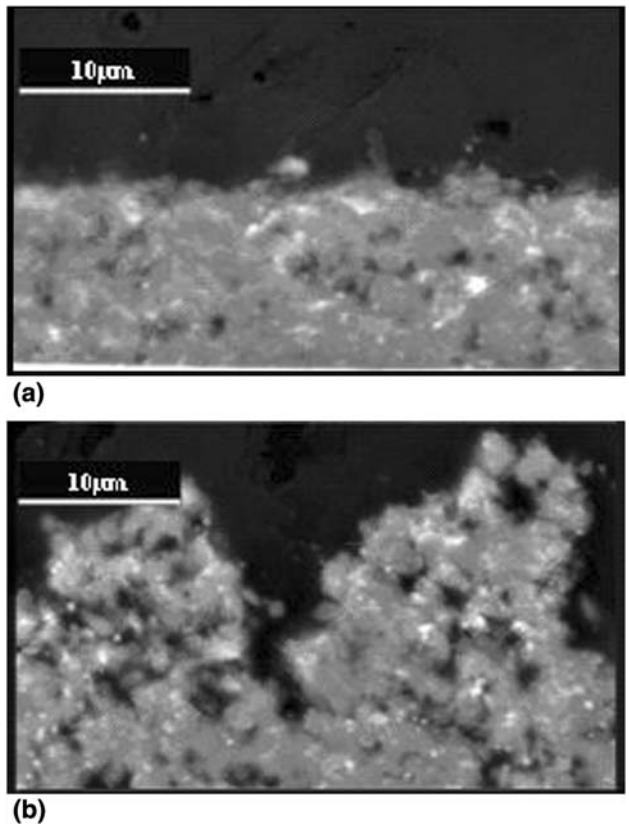

Fig. 12 Al_2O_3-ZrO_2 composite layers showing different microstructures according to the spray parameters: (a) Ar-He 30-30 L min^{-1}, $\bar{h} = 12$ MJ kg^{-1}, SD = 30 mm, SV = 1 m s^{-1}, MP = 10%. (b) Ar-H_2 45-15 L min^{-1}, $\bar{h} \approx 14$ MJ kg^{-1}, SD = 40 mm, SV = 1 m s^{-1}, MP = 10%

the more porous one (Fig. 11b) has been manufactured with a large powder particle size distribution ($d_{90} - d_{10} = 1270$ nm, $d_{50} \approx 500$ nm). Indeed, the particles, depending upon their size, will be submitted to different thermal and kinetic histories. The larger the particle size distribution, the more different the histories and the higher the fraction of poorly treated particles. This leads to the development of the stacking defect density within the coating and to a more porous architecture.

Al_2O_3-ZrO_2 composite coatings (Fig. 12) have been obtained by spraying suspensions with different ratios of alumina to zirconia powders. The relatively dense and homogeneous structure (Fig. 12a) was manufactured with an Ar-He plasma flow (Ar-He 30-30 NL min^{-1}, $\bar{h} = 12$ MJ kg^{-1}) at 30 mm, whereas the more porous and irregular coating (Fig. 12b) was manufactured with an Ar-H_2 plasma gas mixture (45-15 NL min^{-1}, $\bar{h} = 14$ MJ kg^{-1}) at a spray distance of 40 mm. Differences in coating structures result from the combination of two phenomena. First, using H_2 as secondary plasma forming gas leads to arc voltage fluctuations of large amplitudes, as already mentioned. Once again, the available energy in the plasma flow fluctuates together with the voltage fluctuations, so that the different steps in suspension processing (liquid fragmentation, solvent vaporization and solid particles melting and acceleration) are not achieved at the same rates all along the time of flight of the feedstock and consequently the *U* and *R* typified features increase within the coating. Second, when the spray distance increases, the quantity of poorly treated particles increases. This phenomenon is emphasized by arc voltage fluctuations. This leads to more porous coatings with irregular architectures. In this case, the effect of spray distance appears predominant in regard to other operating parameters. As a consequence, using an Ar-He plasma gas mixture allows more homogeneous particle processing; meanwhile, the heat transfer to particles is less efficient (a_φ coefficient is lower) than that of Ar-H_2 plasma gas mixture.

At last, the Al_2O_3-ZrO_2 finely structured multilayers (Fig. 13) have been manufactured with two plasma gas mixtures and two spray distances by alternating the injection of two suspensions of Al_2O_3 and ZrO_2. The denser coating (Fig. 13a) results from the use of an Ar-H_2 plasma gas mixture (45-15 L min^{-1}, $\bar{h} = 14$ MJ kg^{-1}) and at a spray distance of 30 mm, whereas the porous coating (Fig. 13b) results from the use of an Ar-He plasma gas

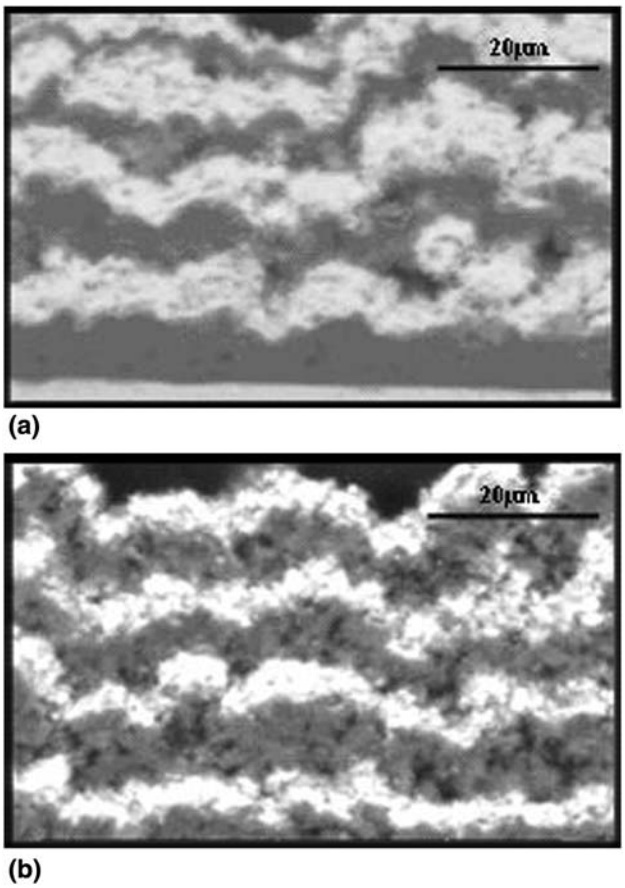

Fig. 13 Al_2O_3-ZrO_2 finely structured multilayers showing different microstructures according to the spray parameters (SV = 1 m s^{-1}, MP = 10%): (a) Ar-H_2 45-15 NL min^{-1}, $\bar{h} = 14$ MJ kg^{-1}, SD = 30 mm (''dense''). (b) Ar-He 30-30 NL min^{-1}, $\bar{h} = 12$ MJ kg^{-1}, SD = 30 mm (''porous'')

mixture (30-30 L min^{-1}, $\bar{h} = 12$ MJ kg^{-1}) and a 30 mm spray distance. In this case, and opposite to composite layers manufacturing (where spray distance was varied), the effect of the plasma gas mixture appears predominant (since the spray distance is kept constant), whereas the effects of arc voltage fluctuations are minored (due to the shorter spray distance). As a consequence, using an Ar-H_2 plasma gas mixture allows in this case a more efficient particle processing (once again, meanwhile arc voltage fluctuations exhibit higher amplitudes) because of the better quality of thermal transfer to particles (a_φ coefficient is higher). Also, one could assume that layer consolidation/densification takes place during coating manufacturing due to the higher heat flux imparted by the plasma flow to the substrate (φ_s value is higher) and since characteristic times between particle solidification (in the order of 10^{-6} s) and the torch/substrate interaction (in the order of 10^{-2} s) are significantly different; that is, most of the heat flux imparted by the plasma flow is transferred whereas the particle is in a solid state.

5. Conclusion

The main characteristics of the plasma flow used to process the suspension droplets have been approximated by means of an analytical model describing the torch operating conditions according to the specific enthalpy at the nozzle exit and the gas thermophysical properties. This control associated with the study of the evolution of spray beads according to the operating conditions enabled to better understand the effects of spray parameters and their interdependences, particularly the influence of the plasma flow through its ability to transfer its thermal and kinetic energies and the one of the spray distance which is more critical in the SPS process compared to the APS one.

According to the gas composition, the plasma flow will present different thermophysical properties, leading to different processings of the suspension and so the manufacturing of coatings with different characteristics.

Thus, several coatings with different architectures have been manufactured in a reproducible way: dense or porous, graded pore level or composition and, at last, Al_2O_3-ZrO_2 finely structured multilayers.

References

1. P. Fauchais, R. Etchart-Salas, V. Rat, J.-F. Coudert, N. Caron, and K. Wittman-Teneze, Parameters Controlling Liquid Plasma Spraying: Solution, Sol or Suspension, *J. Therm. Spray Technol.*, 2008, **17**(1), p 31-59
2. X. Chen, Heat and Momentum Transfer Between a Thermal Plasma and Suspended Particles for Different Knudsen Numbers, *Thin Solid Films*, 1999, **345**(1), p 140-145
3. P. Fauchais, V. Rat, J.-F. Coudert, R. Etchart-Salas, and G. Montavon, Operating Parameters for Suspension and Solution Plasma-Spray Coatings, *Surf. Coat. Technol.*, 2008, **202**, p 4309-4317
4. O. Tingaud, A. Grimaud, A. Denoirjean, G. Montavon, V. Rat, J.-F. Coudert, P. Fauchais, and T. Chartier, Suspension Plasma-Sprayed Alumina Coating Structures: Operating Parameters vs. Coating Architecture, *J. Therm. Spray Technol.*, 2008, **17**(5-6), p 662-670
5. C. Delbos, J. Fazilleau, V. Rat, J.-F. Coudert, P. Fauchais, and B. Pateyron, Phenomena Involved in SPS—Part 2: Zirconia Particle Treatment and Coating Formation, *Plasma Chem. Plasma Process.*, 2006, **26**(4), p 393-414
6. V. Rat and J.-F. Coudert, A Simplified Analytical Model for d.c. Plasma Spray Torch: Influence of Gas Properties and Experimental Conditions, *J. Phys. D*, 2006, **39**, p 4799-4807
7. F.-I. Trifa, G. Montavon, and C. Coddet, Model-Based Expert System for Design and Simulation of APS Coatings, *J. Therm. Spray Technol.*, 2007, **16**(3), p 128-139
8. E. Pfender, Thermal Plasma Technology: Where Do We Stand and Where Are We Going? *Plasma Chem. Plasma Process.*, 1999, **19**, p 1-31
9. L. Xie, X. Ma, A. Ozturk, E.H. Jordan, N.P. Padture, B.M. Cetegen, D.T. Xiao, and M. Gell, Processing Parameter Effects on Solution Precursor Plasma Spray Process Spray Patterns, *Surf. Coat. Technol.*, 2004, **1**(183), p 51-61
10. K. Burm, W.J. Goedheer, and D.C. Schram, The Isentropic Exponent in Plasmas, *Phys. Plasmas*, 1999, **6**, p 2622-2627
11. M.-P. Planche, J.-F. Coudert, and P. Fauchais, Velocity Measurements for Arc Jets Produced by a d.c. Plasma Spray Torch, *Plasma Chem. Plasma Process.*, 1998, **18**, p 263-283
12. R. Etchart-Salas, ''Atmospheric Plasma Spraying of Submicron-Sized Solid Particles in Suspension. Experimental and Analytical Approach of Involved Phenomena in Reproducibility and

Quality of Coatings,'' Ph.D. Thesis, University of Limoges, France, 2007 (in French)
13. R. Etchart-Salas, V. Rat, J.-F. Coudert, P. Fauchais, Assessment of Thermal Flux Transferred by a Plasma Spray Torch on a Substrate at Short Stand-Off Distances, *Proceedings of Actes du Congrès Français de Thermique – Défis Thermiques dans l'Industrie Nucléaire, Ile de Ré*, F. Penot, M. El Ganaoui, D. Petit, and P. Fauchais, Ed., May 16-19, 2006 (Paris, France), Société Française de Thermique, 2006, p 733-738 (in French)